archives
of thermodynamics
Vol. **44**(2023), No. 4, 535–562
DOI: 10.24425/ather.2023.149733

Determination of an axial gas cyclone separator cut-off point by CFD numerical modeling

ARKADIUSZ RYFA[a*]
MIESZKO TOKARSKI[a, e]
WOJCIECH ADAMCZYK[a]
ADAM KLIMANEK[a]
PAWEŁ BARGIEL[a]
RYSZARD BIAŁECKI[a]
MICHAŁ KOCOT[b]
MARIAN NIESLER[c]
HARALD KANIA[c]
JANUSZ STECKO[c]
MARIANNA CZAPLICKA[d]

[a] Silesian University of Technology, Institute of Thermal Technology, Konarskiego 22, 44-100 Gliwice, Poland

[b] ArcelorMittal Poland, al. Piłsudskiego 92, 41-308 Dąbrowa Górnicza, Poland

[c] Institute for Ferrous Metallurgy, Łukasiewicz Research Network, Karola Miarki 12, 44-100 Gliwice, Poland

[d] Institute of Environmental Engineering, Polish Academy of Sciences, Marii Skłodowskiej-Curie 34, 41-819 Zabrze, Poland

[e] AGH University of Science and Technology, Department of Fuels Technology, Czarnowiejska 30, 30-059, Kraków, Poland

Abstract This paper deals with the numerical simulation of a pilot-scale axial cyclone separator. The main purpose of this paper is to develop a numerical model that is able to foresee the cyclone separator cut-off point. This is crucial in blast furnace gas installation to capture large particles containing carbon and iron, while allowing smaller particles such as zinc and lead to pass through. The cut-off point must be designed to give a suf-

*Corresponding Author. Email: arkadiusz.ryfa@polsl.pl

ficiently high zinc and lead content in the sludge created after the second cleaning stage. This allows the sludge to become a commercial product. To design this cut-off point, an investigation of the influence of inlet gas velocity, temperature, and the angle of guiding vanes at the inlet was done. The developed CFD model was validated against experimental data on the fractional efficiency of the cyclone separator. The results were in good agreement with the experimental data for all parameters tested. The behavior of the particles inside the cyclone was also physically correct.

Keywords: CFD; Cyclone separator; Dust; Blast furnace; Zinc; Cut-off point

1 Introduction

A cyclone separator is a device that uses centrifugal force to separates solid particulates from swirling fluid [1]. Its biggest advantages are simple construction, low maintenance and operational costs, low pressure loss, and usability in difficult operating conditions such as high pressure and temperature. Cyclones can be readily scaled to virtually any mass flow. There are two main types of cyclones, which differ in the method of swirling the gas: axial and tangential. The former has a gas inlet axially located on the top wall and uses guiding vanes to enforce the swirl. A tangential cyclone has an inlet (or inlets) located on the side wall, and the gas is swirled by sliding along the side wall. Both types have to be designed for a specific gas velocity, dust composition, and desired separation efficiency. However, it is possible to alter the separation efficiency of both designs. For the axial construction, the angle of the guiding vanes can be changed, whereas for the tangential one, there are shutters mounted in the inlet channels, which can increase the inlet velocity. For small constructions, this tuning can be done while the cyclone separator is running, but for large constructions, this requires a break in operation.

Cyclones are widely used in industry to separate solid material from a gaseous [2] or liquid phase, in circulating fluidized bed boilers for combustible particle separation [3] and in steel plants for gas cleaning [4] just to name a few applications. The gas flow inside a cyclone separator consists of two vortexes [5]: the outer vortex is located on the side wall of the device, and the gas spirals downward. There, large enough particles slow down and finally slide down to the ash hopper. The second vortex is an ascending one located around the center axis, and it directs the cleaned gas to flow toward the so-called vortex finder, which is an outlet of the cyclone. Such a com-

plex flow may pose a challenge when an attempt is made to build a correct numerical model. Cyclone operation is often analyzed via experiments. Hsu *et al.* [6] tested a variety of geometrical configurations and rated their performance using a quality factor. In this study, a quality index is given as a function of the main geometrical parameters. The particle dynamics and trajectories were experimentally analyzed by Roloff *et al.* [7]. Celis *et al.* [8] investigated the effect of swirl vanes and vortex stabilizers on the flow of a cyclone. The effect of the geometric configuration of the inlet on the collection efficiency and noise of an axial flow cyclone was evaluated by Babaoglu *et al.* [9]. The influence of an apex cone on the flow inside an axial cyclone was investigated by Zhang *et al.* [10], whereas Yoshida [11] investigated the influence of an apex cone on the separation of fine particles. Others, such as Yang *et al.* [12] tested the influence of operating conditions (velocity, temperature) on the performance of a cyclone separator. Such papers have great value because they can provide data for the validation of numerical models. Nowadays, computational fluid dynamics (CFD) is often used to test new cyclone constructions or to test the performance of cyclones under various conditions. Huang *et al.* [13] used CFD to test the performance of a cyclone with a slit on the conical part. Zheng investigated the influence of a shunt device on cyclone performance [14]. Pandey and Brar [15] used numerical modeling to test the behavior of cyclones with different shapes of the conical section. An analysis of the effect of the cross-sectional shape of the inlet on the performance of a multi-inlet gas cyclone was performed by Babaoglu *et al.* [2]. CFD is also used to foresee the influence of geometrical modifications on cyclone operation [16]. When a cyclone separator cut-off point is needed, CFD is a method of a choice [1]. There, the angle of guide vanes at omnidirectional inlet was adjusted to determine its impact on cut-off point. The CFD model can be supplemented with soft computing methods such as neural networks or deep learning to reduce computational time [17]. The effect of inlet duct angle on the performance of a cyclone was simulated by Wasilewski and Brar [18]. Xiang and Lee [19] tested the influence of the diameter of the exit tube on the flow field, whereas Su *et al.* [20] investigated the effect of the inlet configuration on the performance of a cyclone. The influence of the size of a cyclone on the separation efficiency was investigated by Azadi *et al.* [21]. Oh *et al.* [22] simulated the cyclone for varying internal pressure. Tests of the inlet periodic velocity were performed by Chen *et al.* [23]. CFD combined with genetic algorithms or neural networks is also used to find the optimum dimensions and inlet conditions of cyclones [24]. An important aspect when applying CFD to

the simulation of the flow inside a cyclone is the proper selection of the turbulence model. In some papers [25, 26], various turbulence models such as k-ε, Reynolds stress model (RSM), and large eddy simulation (LES) were tested. For some time, RSM has been a typical choice for modeling cyclones [24]. The results produced by RSM are in good agreement with the experiments, and yet the model is relatively undemanding in terms of mesh and computational effort. The second choice for modeling cyclones is LES [27]. This option can resolve the flow more accurately than RSM, but it consumes more computational resources. When transient turbulence fluctuations are to be considered LES should be used. This approach was applied to find the characteristic of the turbulence of cyclone separator with vortex stabilizer [28]. Some researchers have analyzed cyclones operating in steady state [29] whereas others used transient models [18]. The approach depends on the goal of the model. Here, both approaches were initially used and compared. Eventually, steady analysis was used. In summary, there are many papers on modeling cyclone separators. Various methods and approaches were used for this purpose. Despite this fact, none of the studies determined the reflection coefficients for the particles.

This work is devoted to the development of a numerical model of a pilot-scale axial cyclone separator. The main aim of the CFD model is to foresee the cut-off point of the cyclone separator for actual blast furnace (BF) gas particles. The main objective of the project under which this work has been carried out is to assess the geometry and flow parameters that will allow the separation of $\approx 85\%$ of the dust from BF gas in a large steel plant. These larger particles contain carbon and iron, which are valuable for the pig iron production process. Thus, the separation of large particles from gas will allow iron- and carbon-rich particles to be recycled into the BF, thus saving natural resources (iron) and energy (coke). In addition, the same large particles contain only a small amount of zinc and lead. These elements are present mainly in fine particles and have a negative impact on the quality of the pig iron produced in the furnace. Hence, the recirculation of these particles is undesirable. The role of the cyclone separator is thus to separate the large particles, while the small particles, containing lead and zinc, should be discharged from the device along with the outlet gas [4]. Those fine particles are then removed from the gas, typically in a wet scrubber (WS). When the zinc and lead content of the sludge is high enough, the sludge can be used further as a commercial product [30]. In the long run, because the gas velocity, geometry of the cyclone separator, and mass of the BF dust particles have a major impact on the separation efficiency, a multi-

parameter analysis needs to be carried out, because only proper fractions of the dust should be recirculated (separated). Due to cost considerations, it was decided to use the same dust in the pilot-scale cyclone separator. The model is validated against experimental data for various operating conditions, such as gas velocity and temperature or guiding vanes angle. The long-term goal is to obtain a robust and fast numerical model that can be used for designing a full-scale industrial cyclone separator for a steel plant's de-dusting installation. For this reason, the dust collected in the steel plant is used in the experimental setup, and the operating conditions of the test cyclone separator are close to the full-scale industrial installation. In this study a 3D steady-state CFD model was developed. The model uses the RSM turbulence model and discrete phase model (DPM) approach to model dust particles. These methods have been selected because they allow one to obtain reliable results within a reasonable computation time. The novelty of the proposed approach is the determination of the reflection coefficient that defines the momentum losses during the particle–wall collisions and the splitting of the model into two parts, which speeds up the calculations and allows for the use of a better-quality mesh. Additionally, each dust fraction was injected separately into the cyclone so that it was easy to calculate the fractional separation efficiency and to use the experimental data. The typical approach found in the literature does not mention the selection of the reflection coefficients or assumes a value of 1.

The paper is divided into 5 sections. First is an introduction. Section 2 describes the test rig and the measurements. Next goes CFD modeling (Section 3) and model validation (Section 4). Last section is devoted to conclusions.

2 Experimental rig and measurements

The test rig is shown in Fig. 1 and is presented schematically in Fig. 2. It consists of an air preparation system (including an electrical heater (EH) and a dust dosing device), an axial cyclone separator, a WS, a bag filter system, and a fan. First, ambient air (I) is sucked from the environment and heated by an EH. The heater is controlled by a temperature sensor mounted at the inlet of the cyclone (II) so that the requested operating temperature is maintained. The dust is then dosed with a screw feeder (III). Dust-laden air enters the cyclone separator through the annular tube (diameter 0.196 m), where a portion of the dust is separated and collected at the

bottom of the installation (IV). The part of the cyclone where separation occurs has a height of 0.66 m and a diameter of 0.25 m (cylindrical section). The air containing the remaining dust leaves the cyclone separator through a vortex finder (0.094 m diameter) and flows through the WS and through a baghouse filter. Clean air flows through a fan to the stack (X), while the sludge is removed from underneath the scrubber (VII). Dust separated in the baghouse is collected in (IX).

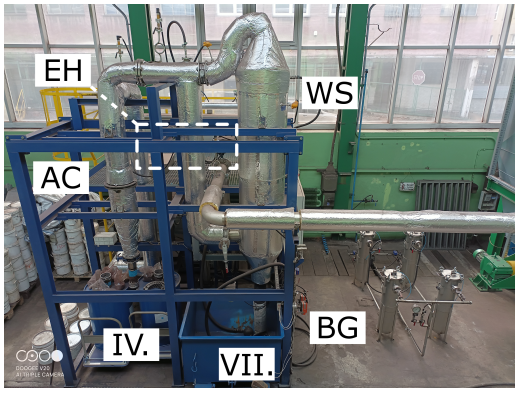

Figure 1: Test rig – general view: EH – electric heater, AC – axial cyclone, WS – wet scrubber, BG – baghouse, VI – collected dust, VII – collected sludge.

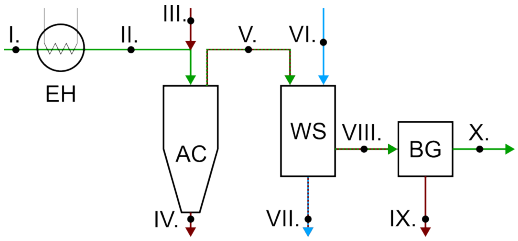

Figure 2: Test rig scheme: EH – electric heater; AC – axial cyclone; WS – wet scrubber; BG – baghouse; measurement points I, II – clean air; III, IV, IX – BF dust; V, VIII – dust laden air, VI – water injection, VII – sludge, X – clean air.

The analysis in this paper is limited to the cyclone separator. The WS is a subject of separate research.

The BF releases gas at a gauge pressure in the range of 0.05 to 0.2 MPa and at a temperature of 373 to 423 K. Although the gas temperature can be easily controlled on a laboratory scale, operation of the test rig at overpressure poses a challenge. First, the amount of air needed in the installation

would require a large compressor and tank to work in a steady state for a longer time. Although this is not essential for the cyclone separator itself, it is essential for the second part of the separation process, which is carried out with a WS. The second issue is that feeding the dust to the compressed gas is problematic, because the dust can escape from the installation, contaminate the environment, and reduce the quality of the determination of the efficiency of the cyclone separator. For these reasons, it was decided to operate the rig at ambient pressure, especially so that the pressure level in the cyclone separator did not affect its operation. The BF gas (present in the real installation) was replaced by ambient air, whose pressure was measured at the inlet to the installation (I) and at the outlet of the cyclone (V) by a piezo-resistance sensor (uncertainty 0.6%). The volumetric flow rate of clean air was measured (I) using an orifice (measurement uncertainty 1%). The temperature of the gas was measured at several locations: at the inlet to the rig (I); at the outlet from the gas heater (II); at the inlet (III); and at outlet (V) of the cyclone by a Pt100 resistance thermometer (maximum uncertainty 0.4 K). Air humidity was measured at the inlet to the rig (I) using an HTDT2500 sensor (uncertainty 2.5%). The dust supplied to the installation was collected from the BF of the steel plant. As seen in Table 1, the mass fraction of the smallest dust (< 0.028 mm) is less than 20%. The average fractions (0.028–0.1 mm) contain approximately 60% of the mass, whereas the remaining part is in larger fractions. The demand to separate 85% of the mass means that the cut-off point for cyclone separation must be located at a fraction below 0.02 mm. The cyclone separator used in the experiments was designed with exchangeable guide vanes (denoted as K1, K2, and K3) that allowed for a change in the swirl angle at the inlet of the cyclone separator. In theory, this was supposed to allow control over the separation efficiency, indirectly impacting the separation cut-off point. This point is especially important, because smaller particles contain harmful compounds that cannot be redirected back to the BF. The zinc content in the dust was determined using an ICP-OES Agilent 5100 SVDV spectrometer. As seen in Table 1, zinc was present mainly in the smallest fractions, where its mass fraction was almost 7% for the smallest particles. The zinc content decreased with increasing particle diameter and for the assumed cut-off point was around 2%.

For larger diameters, the zinc mass fraction was gradually reduced to less than 0.5%. The cyclone separation efficiency is computed as

$$\eta = \frac{\dot{m}_c}{\dot{m}_{\text{in}}}\,, \tag{1}$$

Table 1: Dust fractional composition (%) and zinc mass content (%).

Fraction, mm	ID 4 (8 m/s)	ID 26 (7 m/s)	ID 30 (10 m/s)	Zn content
< 0.0019	6.4	5.2	8.9	6.7
0.0019–0.0037	2.4	2.2	3.1	6.2
0.0039–0.0064	2.1	1.4	2.3	4.2
0.0064–0.0088	2.5	2.3	2.7	3.6
0.0088–0.0124	1.8	1.8	2.0	2.9
0.0124–0.0180	1.7	2.2	1.8	2.5
0.0180–0.0232	0.9	1.0	0.9	2.2
0.0232–0.0277	0.5	0.5	0.5	2.0
0.0277–0.056	17.2	16.0	14.0	1.9
0.071–0.056	8.1	6.8	8.8	1.2
0.1–0.071	13.8	14.6	16.0	0.8
0.16–0.1	22.5	20.8	20.8	0.8
0.2–0.16	7.0	7.6	6.1	0.6
0.315–0.2	9.3	12.6	8.3	0.6
0.4–0.315	2.2	2.8	2.0	0.5
0.63–0.4	1.6	2.0	1.8	0.5
0.8–0.63	0.2	0.3	0.2	0.5
1.6–0.8	0.0	0.1	0.0	0.4
> 1.6	0.0	0.0	0.0	0.0

where m_c (kg/s) is the mass of dust collected from the cyclone ash hopper, and m_{in} (kg/s) is the mass dosed to the installation. All masses are collected for the steady-state operation of a rig for a given measurement. The mass of dust that is fed into the installation can be computed as

$$\dot{m}_{\text{in}} = \frac{m_0 - m_1}{\tau}\,, \tag{2}$$

where m_0 (kg) and m_1 (kg) are the masses on the ash tray of the screw feeder at the beginning and end of the measurement, respectively, and τ is the measurement time (s). The fractional efficiency is calculated in the same way:

$$\eta_{c,f} = \frac{\tau \dot{m}_{c,f}}{(m_0 - m_1)\, c_f}\,, \tag{3}$$

where $m_{c,f}$ (kg) is the mass of the dust of a given fraction collected from the ash hopper, and c_f is the mass fraction of a given fraction from Table 1. ID stands for number of measurement taken.

The dust used in the laboratory installation was a mixture of dust and dried sludge collected in the real BF de-dusting installation. Dust and sludge were mixed in the proportion 3:1 and were sampled to verify whether the particle distribution was the same at all sample locations. The dust collected at the bottom of the laboratory installation cyclone separator (IV) was weighted (accuracy 0.1 g) and fractionated using laser diffraction according to the ISO 13320:2009 standard into fractions ranging from less than 0.056 mm to greater than 1.6 mm. The smallest fractions (i.e., below 0.056 mm) were further split with the use of counterflow in a Bahco high-speed centrifuge. In total, there were 19 fractions, with the smallest fraction below 0.0019 mm. The density of each fraction was determined using the pycnometric method. Each analysis was repeated three times to ensure that the dust analysis was correct. The sludge (VII) collected from the WS outlet was analyzed in the same way but was dried beforehand. The results in Table 1 show the average of three analyses of the dust/sludge mixture. Laboratory tests were aimed at determining the parameters that influence the separation efficiency and providing data for the validation of the numerical model. In total, more than 30 measurements were taken. As seen in Table 2, the gas velocity tested at the entrance of the cyclone separator was between 7 m/s and 13 m/s, which corresponds to the expected velocities in the industrial installation. In addition to gas velocity, the gas temperature, dust content, and swirling angle were also varied. Separation efficiency ranged from 90.4 to 95.2%, depending on the conditions. The tests proved that the temperature and dust content, within the tested limits, did not influence the separation efficiency. To test the impact of the swirling angle on the performance of the cyclone separator, three different flow guide vanes were tested. These vanes produced swirl angles of 21° (K1), 30° (K2), and 39° (K3). Measurements showed that the angle of the guide vanes had some, but not an overwhelming, influence on the cyclone separation efficiency. That is, with increasing angle, the separation efficiency also increased, but only by about 1%. One test (ID 201) was conducted without any vanes (no initial gas swirl). For this case, the separation efficiency dropped to about 67%. This indicated that, although the swirl was necessary, the angle was not a crucial parameter, at least not in the tested angle range. Unlike this, the velocity of the gas affected the separation efficiency of the cyclone separator. With increasing velocity, the efficiency also

increased by about 0.5% per 1 m/s increase in velocity. However, this effect was limited. Although the smallest fractions were almost not captured within the investigated velocity interval, for a velocity above 10 m/s, nearly all larger fractions were separated. Therefore, it was difficult to observe any increase in efficiency between 10 and 13 m/s.

Table 2: Performed measurements of the cyclone. Boxed measurements were chosen for numerical model validation: v_{II} – inlet air mean velocity, T_{II} – air temperature at the inlet, η – separation efficiency of the cyclone.

ID	v_{II}	Flow guide	Dust content	T_{II}	η
–	m/s	–	g/m$_n^3$	°C	%
3	8	K1	15	125	94.4
4	8	K1	15	125	91.5
5	8	K1	15	125	92.6
6	7	K1	15	125	92.7
7	8	K1	15	125	92.2
10	8	K1	15	100	93
11	8	K1	15	150	91.8
19	7	K1	30	125	91.3
23	8	K1	15	125	95.2
25	8	K1	15	125	91.5
26	7	K1	15	125	92.4
27	8	K1	15	125	94.3
28	8	K2	15	125	94.6
29	8	K3	15	125	93.3
30	10	K1	15	125	93.3
31	13.1	K1	15	100	93.9
130	8	K1	15	125	93.9
201	8	–	15	125	66.8
205	8	K1	15	100	92.7
206	10	K1	15	100	93.8
208	10	K1	15	100	94.1
209	13.1	K1	15	100	94.0
210	10	K1	30	125	93.0

For model validation, givens that velocity was the most important parameter that influenced the separation efficiency, three measurement series at different velocities of 7, 8, and 10 m/s were taken. These measurements were denoted as ID 26, ID 4, and ID 30, respectively. Because the performed measurements had very little effect on the swirl angle generated by the flow guides K1, K2, and K3, the measurements (except for two) were executed using the K1 guides.

3 CFD model outline and modeling strategy

The calculations were carried out using the commercial CFD package Ansys/Fluent 19.2. The cyclone separator itself consists of three main parts. The first part is an inlet part with a gas supply pipe. Next, there is the main body part of the cyclone, which consists of flow swirling elements, cylindrical and conical tubes, and the vortex finder. There, the flow swirls, and the dust is separated from the gas. The last part is a vertical gas outflow pipe (where the gas containing the non-separated particles is rejected from the device). The main simplifications of the model considered geometry, where small, unimportant features of a cyclone were neglected. In addition, the analysis was finally run in a steady state to save time and computational effort with a negligible impact on solution quality due to the stabilized flow field. Splitting the numerical model into two parts allowed for significant savings in terms of computational time and resources. The inlet zone required a finer mesh and was needed just to generate velocity and particle profiles at the cyclone inlet. The cyclone, on the other hand, with coarse mesh required much longer computational time to stabilize the solution.

A 3D Reynolds-averaged Navier-Stokes formulation of the governing equations was used. The RSM turbulence model was applied based on the scalar dissipation rate (ε) with a linear pressure strain. A standard approach proposed in Fluent was used to model turbulent diffusive transport with scalar turbulent diffusivity. Since all the model constants were default, then in linear pressure strain slow pressure strain term used 1.8 as a constant while rapid pressure strain used 0.6. The wall boundary condition was taken from the kinetic energy equation. The wall reflection term was modelled with $C_1' = 0.5$, $C_2' = 0.3$ and $C_\mu = 0.09$. The dissipation rate constants were 1.44 and 1.92. Scalable wall functions were also used due to the Y_+ range of 5.5 to 127. Detailed equations can be found in Section 4.10 of the Ansys Manual [31].

There were three unknown parameters when setting up the mathematical model of the cyclone separator:

- the reflection coefficients, defining the momentum losses during the particle–wall collisions;
- the profile of the inlet velocity;
- the distribution of the particles at the inlet.

The reflection coefficients depend on the properties of the dust and the type and condition of the cyclone separator material. They are extremely difficult to measure, so they were discovered by adjusting the simulation results to those of the experiments. Because the same dust will be used in both the full-scale and laboratory installation, the values obtained in the latter can then be used in the former.

The intersection of the straight outlet and curved inlet pipes produces an unsymmetrical profile of the inlet velocity and a non-uniform distribution of the particles at the inlet of the cyclone separator. Additionally, this distribution differs between fractions of particles. To obtain realistic boundary conditions at the inlet of the cyclone separator, the computational domain was extended by the inlet pipe, as shown in Figs. 3 and 5. To reduce the size of the numerical model of the cyclone separator and the simulation time of parametric studies, the computational domain was divided into two parts separated by a plane (D) (see Fig. 3). An additional advantage of

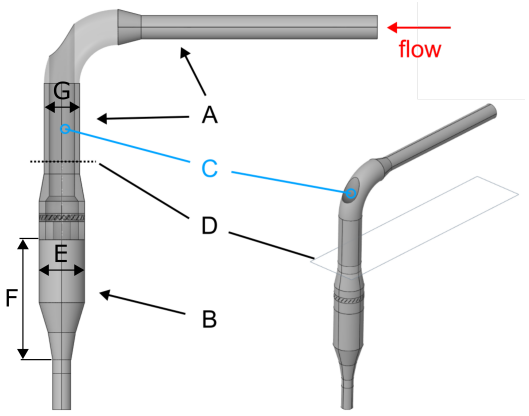

Figure 3: Computational domain: A – inlet zone, B – cyclone, C – outlet pipe, D – split plane, E – diameter of cylindrical part (0.25 m), F – height of the cyclone (0.66 m), G – diameter of inlet pipe (0.196 m).

this approach was the possibility of using a high-quality regular mesh in the cyclone separator. Due to the complex velocity pattern in this device, the choice of an appropriate mesh was of special importance. To verify the correctness of such an approach, one simulation was run iteratively. That is, both the inlet section and the cyclone simulation were run, and velocity and pressure fields were passed between them. The results of such an analysis showed no significant influence of a pressure field generated in the cyclone on the velocity distribution calculated in the inlet section.

The first zone consists of the inlet pipe (A), whereas the second comprises the main body of a cyclone (B), as indicated in Fig. 3. Both zones were solved independently and coupled by a velocity and pressure boundary conditions. The outlet velocity and particulate distribution of zone A were treated as an inlet condition to zone B. The simulations were carried out in steady-state using a pressure-based solver with gravity on. The RSM was used to model turbulence.

Next, steady-state and transient analyses of the flow conditions inside the cyclone separator were performed, and the results were compared with the experimental data (series denoted as ID30). For both models, the setup was the same. In the transient analysis, however, a 0.00013775 s time step was chosen with 10 iterations per time step. Furthermore, the data sampling interval was set to 10 time steps. In our case, however, it was a much shorter period (0.135 s), because this particular study was carried out only to validate the steady-state flow field. It confirmed that, the appropriately stabilized steady-state flow field is identical to the costly time-averaged one. The calculated velocity fields are shown in Fig. 4(b). Both profiles were almost identical (which confirms that steady-state and transient led to essentially the same results), except for slight irregularities (flow oscillations) present in the steady-state. In Fig. 4(a), the fractional separation efficiency is presented and it can be stated that both formulations agreed satisfactorily well with the experimental data. The only noticeable discrepancy concerned the fraction 3.9 µm, where the separation efficiency should be around 82% (experiment), whereas numerical models indicated lower values (i.e., $\approx 70\%$ and $\approx 48\%$) according to the steady-state and transient analyses, respectively. Generally, good agreement between the two models indicated that slight flow oscillations in the steady-state analysis did not significantly impact particle behavior. At the same time, steady-state analysis was much less demanding in terms of computational time and resources. Thus, steady-state analysis was chosen for further analysis.

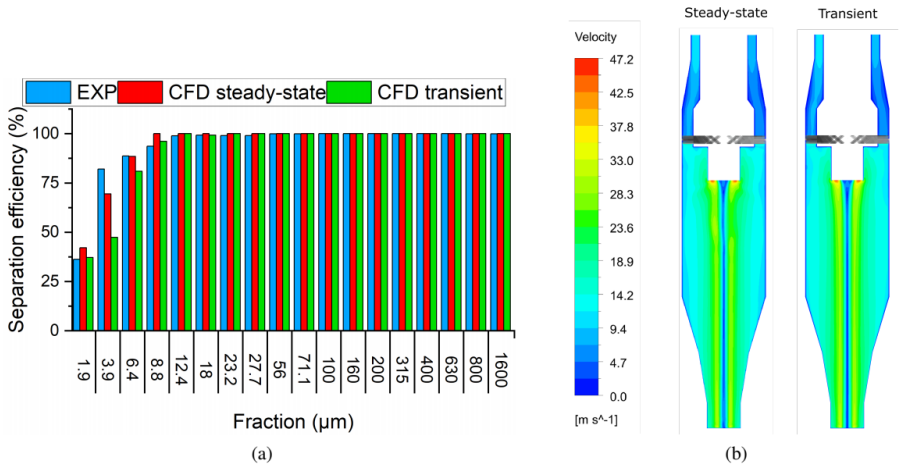

Figure 4: Case ID30 – comparison of the steady-state and transient analysis: a – fractional separation efficiency from experiments (EXP), steady-state (CFD steady-state), and transient (CFD transient) analysis; b – velocity profile provided by the steady-state (left-hand side) and transient (right-hand side) analysis.

3.1 Model description

The setup of both models, (A) and (B), was the same and covered the *Coupled* pressure velocity coupling scheme, QUICK spatial discretization of momentum, turbulent kinetic energy, turbulent kinetic dissipation rate, Reynolds stresses, and energy. PRESTO! was used for pressure discretization. The QUICK scheme was used to improve the stability of the solution and the flow field. Second-order schemes are considered sufficient in most cases, but in this particular case, it was decided to go with the QUICK. The reason behind this is that this scheme offers slightly better stability. This was particularly important to avoid costly time-dependent analyses. The higher order scheme also brings disadvantages, such as, for example, more difficult model convergence. The model was considered converged when all residuals stabilised at an appropriate level. This was below 10^{-3} for continuity and 10^{-4} for velocity and turbulence. Additionally, velocity pressure and mass flux at the outlet were monitored and calculations were terminated when the values at that point did not change.

Because the test rig was located in an enclosed space and the entire piping system with the cyclone separator was insulated, the thermal boundary condition of all model walls was zero heat flux. Particulate matter was

modeled with the discrete phase model (DPM). The particles were tracked with a maximum number of steps of 350 000 and a step length factor of 5. A spherical drag law was enabled for momentum exchange, and a discrete random walk model was enabled with 5 tries and a 0.15-time scale constant. There were 18 separate injections, one for each fraction. With each injection, a constant particle diameter was set equal to the maximal size in the fraction (i.e., for fraction 56 µm, the diameter was 56 µm). The particle type was inert, with a density provided by the measurements. Because the dust content in the gas was low (15 g/m^3_n), the interactions between particles were neglected. Moreover, the interaction between the particles and the gas was limited only to the influence of the gas flow on the movement of the particles, whereas the interaction in the opposite direction was disregarded (one-way interaction).

3.2 Inlet zone

The inlet zone is a curved pipe consisting of a straight run-up section of length ten internal diameters of the pipe; a curved section that intersects with the outlet pipe (presented in Fig. 5); and a straight annular section up to the plane (D), where the pipe model was separated from the geometry of the cyclone separator.

In the industrial gas cleaning installation, the flow is induced by BF gas, which has a higher pressure than ambient air. For technical reasons, gas flow was kept under pressure at the outlet, which, for the pilot installation,

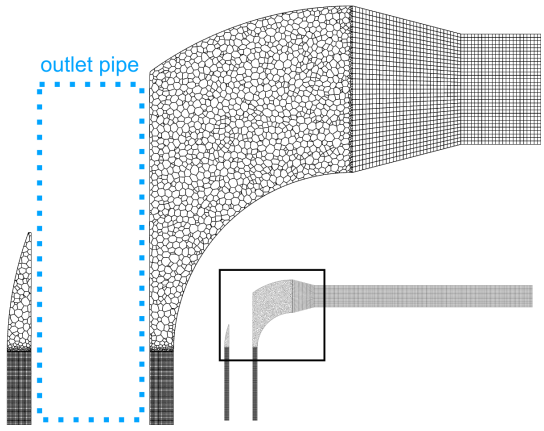

Figure 5: Numerical mesh of the inlet zone at axial cross-section: dotted line – outlet pipe.

was much easier to implement. Because an incompressible model of the gas was employed, the results practically did not depend on the pressure level. The inlet boundary condition (at the entrance of zone A) was set as uniform velocity and temperature with uniformly distributed solid particles.

For the grid independence study, four different grids were tested: 0.25, 0.6, 1.4, and 2.35 mln elements. Dynamic pressure was the parameter observed at the outlet of the zone. The independence study showed that grids with 1.4 and 2.35 mln elements produced very similar results, and the latter was taken for further computations. The final mesh of the inlet zone, being the result of the mesh independence analysis, is presented in Fig. 5 and consists of 2.35 mln elements. Both straight sections were meshed with hexahedral elements, whereas for the curved section, polyhedral elements were used. The minimum orthogonal quality was 0.25, and the maximum aspect ratio was 12.7.

The velocity field in the inlet zone for ID26 is shown in Fig. 6. As shown, a uniform profile was applied at the A.1 inlet. The flow develops throughout the first straight section and then encounters the outlet pipe in the curve region where the profile drastically changes. The velocity profile at the outlet A.2 results from the geometry and is non-uniform.

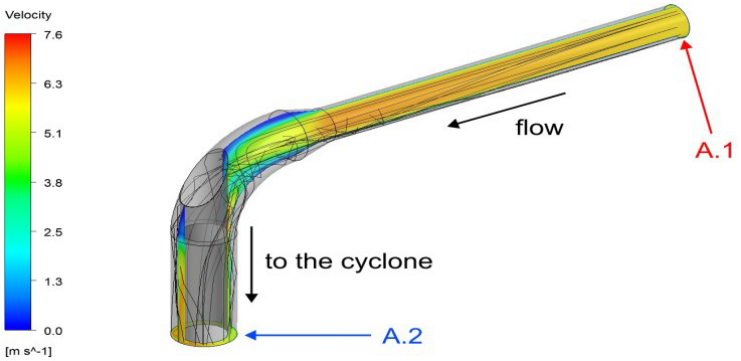

Figure 6: Inlet zone – velocity field and exemplary BF dust trajectories: A.1 – inlet to the inlet zone, A.2 – outlet (inlet to the cyclone).

Several BF dust particle trajectories are also shown as thin black lines. All particle fractions were injected at the A.1 inlet. Some of the heavier particles fell in a straight section and began to bounce off the walls, while the lighter particles remained airborne and continued to move with the airflow. At the A.2 outlet, the intersection coordinates of each particle along with its diam-

eter, density, temperature, flow rate, and velocity components were sorted by diameter and written in text files. This was done automatically using a user-defined function based on the DEFINE_DPM_OUTPUT macro. The files were then read by the cyclone separator model.

The distributions of three BF dust fractions: 3.9, 100, and 800 µm at the A.2 outlet are presented in Fig. 7 for two cases: ID30 and ID26. Case ID30 was characterized by a higher overall mean velocity (higher air flow rate) of approximately 10 m/s, whereas case ID26 corresponded to about 7 m/s. One can see that the gas velocity was always higher at the outer bend of the inlet pipe. The difference between the velocity on the outer and inner sides of the outlet from the inlet zone was about 20%. It became evident that the velocity, combined with the shape of the inlet zone, according to the numerical study, had a serious impact on the distribution of some particles – in this case it was fraction 100 µm, but it also applied to other neighboring fractions. This fraction had a highly non-uniform distribution, where particles tended to aggregate on the inner side of the channel (low-velocity zone), especially visible in the ID26 case. However, smaller dust particles were not affected by the flow and were almost evenly distributed throughout the outlet surface regardless of the gas velocity. The same applied to the largest particles. Wall reflections did not seem to affect the heavy particles' distribution as much as the average one.

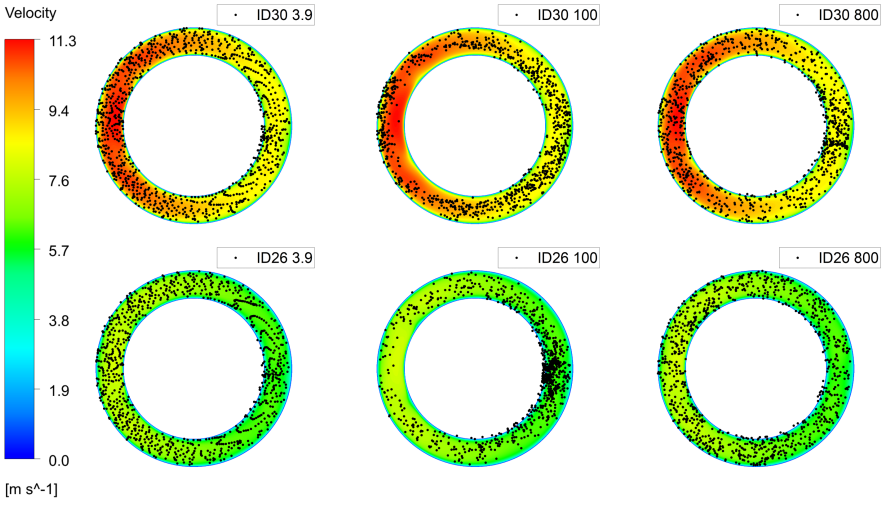

Figure 7: Inlet zone (D-D split plane) – velocity field of cases ID30 and ID26 along with particle distributions of three different fraction: 3.9 µm, 100 µm, and 800 µm.

3.3 Cyclone separator

The detailed geometry of the numerical model is shown in Fig. 8. This covers part of the straight inlet pipe starting from the D split plane (for initial development of the flow profile) and the cyclone separator up to the shutoff valve (6) below the conical part. As dust-laden air (a–b) enters the separator, the annular inlet extends slightly. Then, the airflow is swirled by the flow guides (5) and enters the cyclone, where the separation takes place. The dust particles eliminated from the flow (c) are collected in the dust hopper connected to the cyclone separator through the valve (6).

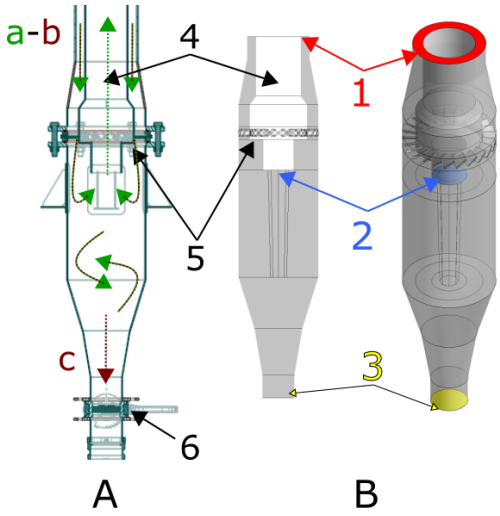

Figure 8: Axial cyclone separator: A – geometry, B – computational domain; a-b – dust laden air, c – captured dust, 1 inlet, 2 – outlet, 3 – particle trap, 4 – outlet pipe, 5 – flow guides, 6 – shut-off valve.

There are three main boundary conditions associated with the computational domain: (1) velocity inlet, (2) pressure outlet, and (3) wall (particle trap). The inlet consists of a velocity profile and a spatial distribution of particles as calculated in zone A. Each dust fraction is applied as a separate injection.

The mesh sensitivity study covered four different mesh sizes ranging from 0.56 to approximately 3 mln elements. These were tested in terms of the predicted velocity profile presented in Fig. 9, where the tangential velocity in the cylindrical zone is shown. The coarsest mesh (0.56 mln el.) appeared to be insufficient, because the maximum velocity near the axis (at 0 m) was

noticeably underestimated when compared with other meshes. Therefore, the second coarsest mesh (0.88 mln el.) was chosen for further simulations, because it produced comparable results to the ones provided by the finer meshes.

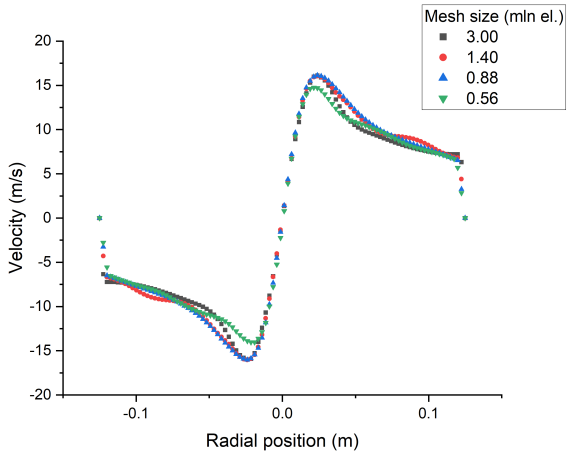

Figure 9: Mesh analysis – comparison of tangential velocity for the tested meshes.

In the next step, courant flow number (CFN) analysis was necessary, because the analyses were performed in a steady state. Such calculations are more robust (which was an important factor during the project) than the transient ones, and the final (averaged) results are the same. However, the computational issues of the steady-state analysis had to be overcome by adjusting the CFN from the default value (200) to 10, which improved the flow stability and convergence. Then, the coarsest mesh providing consistent results was chosen for further calculations, and it was (again) a mesh (0.88 mln) consisting of fully hexahedral elements. The maximum aspect ratio was 4.01. The minimum element quality was 0.45, whereas the maximum skewness was 0.60. The mesh is presented in Fig. 10. On the left-hand side, an axial cross-section is shown throughout the cyclone separator. The normal cross-section A–A is located slightly below the outlet, where an octagonal shape can be observed in the center. This shape improved the quality of the mesh (smoother transition, better structure, similar element size) in the ascending vortex zone. On the right-hand side, a detailed view of the conical part is shown, where the mesh is vertically refined to keep the element's aspect ratio and structure similar.

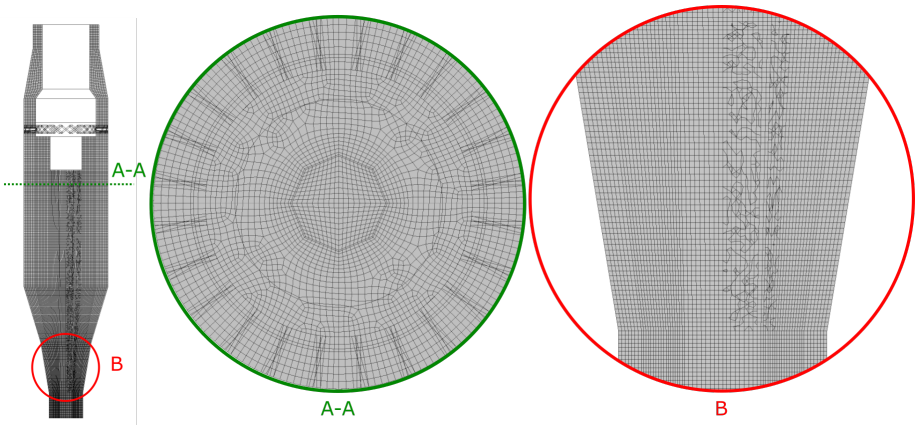

Figure 10: Cyclone separator – final mesh: A – mesh in cross-section, B – detailed mesh in conical part.

Once the mesh was selected, an appropriate value of CFN was required for further stabilization and convergence control of the solution. The impact of four CFN values was investigated: 5, 15, 25, and 35. In all cases, the velocity fields (shown in Fig. 11) and the residuals (not shown) were monitored. At this point, a uniform velocity profile at the inlet was applied; the geometry was axisymmetric, so the velocity field is expected to be symmetric with a low-velocity zone along the axis. As shown, the most symmetrical profile had clearly outlined regions of low velocity (in the axis) below 4.1 m/s, high velocity (in the vicinity of the axis) above 28.7 m/s, and medium velocity (near the wall) between 8.2 and 20.5 m/s with CFN = 15. In the profile for CFN = 5, some minor instabilities were observed, whereas the profiles for CFN = 25 and CFN = 35 were significantly asymmetrical, and the low-velocity region was blurred and even almost completely disappeared. Therefore, CFN = 15 was used in all subsequent calculations.

Once a value of the CFN is established, the reflection coefficients (tangent and normal) need to be determined. The reflection coefficient takes a value between 0 and 1, where 0 stands for no momentum retention and 1 for full momentum retention during the collision of the particle with the wall. The extreme situations, where the particle fully retains or loses momentum, are theoretically possible but not in real application. Therefore, the values 0 and 1 were not considered in the study. Reflection coefficients were chosen according to the separation behavior of the dust measured on the test rig. That is, different pairs of values (tangent and normal) were

tested numerically (from the range 0.1–0.9) using the dust (provided by the experiments). Then, one pair that gave the best fit with the experimental separation, has been chosen and used throughout the model. The coefficients are presented in Table 3, and the chosen pair is given in the box for better clarity. The value of the tangent and normal reflection coefficient was incremented by 0.1 in the range from 0.1 to 0.9. The separation efficiency, calculated as the ratio of trapped (separated) trajectories to all trajectories, was then determined for three different fractions: 3.9, 100, and 800 µm. The chosen fractions covered small, medium, and large particles, because the behavior of particles in the flow depends on mass. The tested reflection coefficients are presented in Table 3, organized in a matrix-like form, and were assumed to be constant. Fractional separation efficiencies are also given (in %). The analysis left two pairs of coefficients that suited the measurements: 0.7–0.8 and 0.8–0.8. The values of the 0.7–0.8 pair are boxed to show that they matched the measurement-based separation efficiencies most closely. Therefore, the reflection coefficients 0.7–0.8 (tangent and normal, respectively) were used in further calculations.

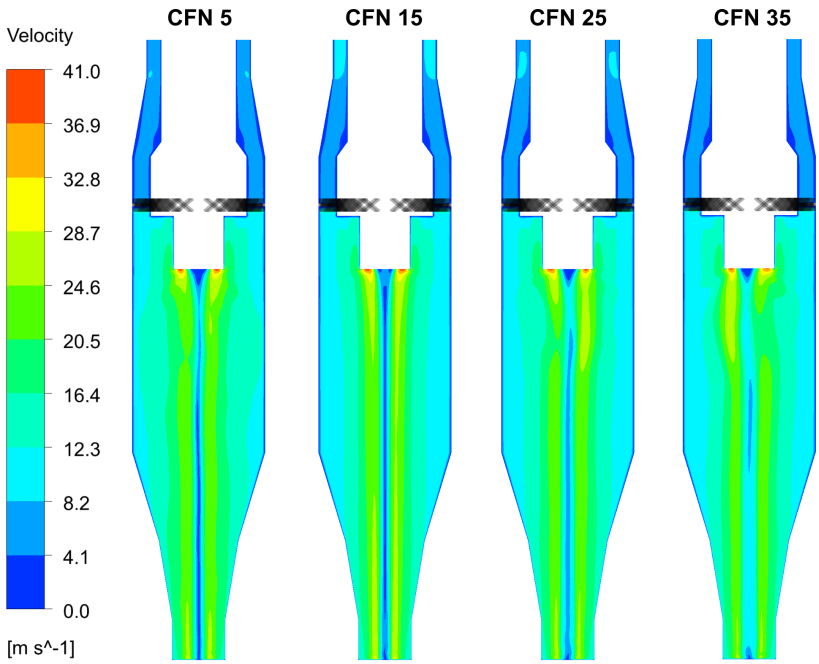

Figure 11: Cyclone – CFN impact on the velocity field (for an axial cross-section).

Table 3: Fractional separation efficiency (%) in terms of different reflection coefficients (values in the box – the best fit with experimental fractional efficiency).

Fraction, (µm)			Reflection Coefficient: Tangent					
			0.1	0.5	0.6	0.7	0.8	0.9
3.9	Reflection Coefficient: Normal	0.1	54.74					53.68
		0.5		55.79			55.79	52.63
		0.6						
		0.7					56.84	
		0.8		55.79	57.89	61.05	57.62	56.84
		0.9	59.29					55.79
100		0.1	100.00					100.00
		0.5		100.00			100.00	100.00
		0.6						
		0.7					100.00	
		0.8		100.00	100.00	100.00	100.00	100.00
		0.9	100.00					100.00
800		0.1	100.00					100.00
		0.5		100.00			100.00	100.00
		0.6						
		0.7					100.00	
		0.8		100.00	100.00	100.00	100.00	100.00
		0.9	100.00					100.00

4 Model validation and discussion

Once the correct CFN value for the model was found, the calculations were performed for three test cases: ID4, ID26, and ID30, which corresponded to three different gas velocities at the input: 8, 7, and 10 m/s, respectively. The numerical model was validated in terms of fractional separation efficiency, but the velocity field needed to be evaluated first. In Fig. 12, the velocity fields of all tested cases are presented. The slightly distorted symmetry of all the profiles was important, yet this was expected since the velocity profile at the inlet is asymmetric. The low velocity region near the axis, as well as the neighboring high-velocity region, is clearly visible. Hence, no anomalies in the velocity field were observed.

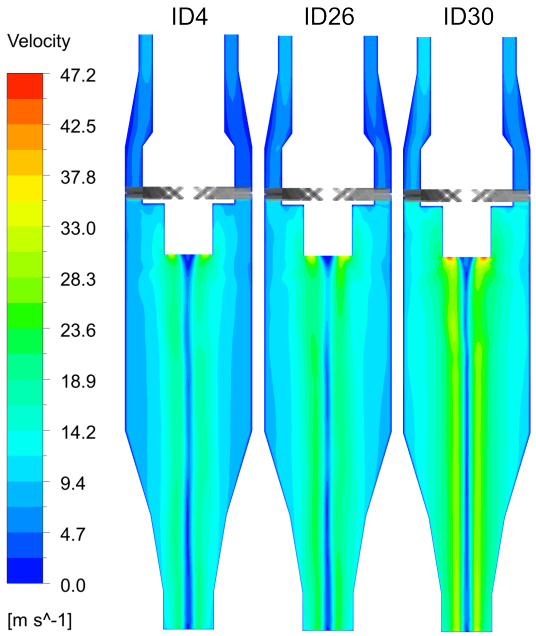

Figure 12: Cyclone separator – velocity field for the validation cases (for CFN = 15).

The predicted behavior of particles with a diameter of 3.9, 100, and 800 µm for a gas velocity of 10 m/s is shown in Fig. 13. For the sake of clarity, only a small number of particles are shown. The 3.9 µm particles moved chaotically, making many laps around the circumference of the cyclone separator. Some of the particles fell into the ash hopper, whereas others reached the internal ascending vortex and left the cyclone separator with the gas. The trajectories of larger particles with a diameter of 100 µm were much more orderly arranged while moving around the cyclone separator. Their trajectories were concentrated near the external walls. Here, all of the particles were separated because they were too heavy for an internal ascending vortex to lift them toward the outlet. The same was observed for the 800 µm particles. However, the trajectories were much steeper in the cylindrical part, while the conical part was crowded (similar to the 100 µm case). It should be noted that, according to the model, the residence time was longer for heavier particles by approximately 2–4 times.

The separation efficiency for each of the measured 18 dust fractions was then compared with the CFD results, which are presented in Fig. 14. Red bars indicate fractional separation efficiencies provided by the CFD model,

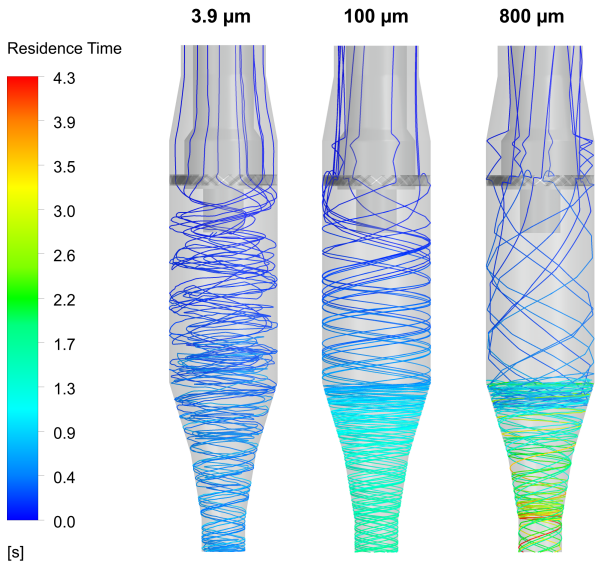

Figure 13: Cyclone separator – predicted particle trajectories and their residence time.

whereas blue bars represent experimental efficiencies. The separation efficiency of the CFD model was calculated as a ratio of the number of trajectories of a given diameter captured at the bottom of a cyclone separator (the particle trap in Fig. 3) to the number of injected trajectories at the inlet of the cyclone separator. For the measurements, the fractional separation efficiency was calculated using Eq. (3). When analyzing the results of the fractional efficiency (see Fig. 14), strange behavior associated with the fraction 56 µm was observed. While the efficiencies changed continuously for other fractions, there was a jump in efficiency for the fraction 56 µm. This can be explained as follows: First, as already mentioned, the sieve analysis was performed on two different devices. The coarse fractions were separated using a laser diffraction device whose smallest sieve was of 71 µm mesh diameter. The mass of the dust leaving this device was transported to a lab located in another city. Here, the counterflow Bahco high-speed centrifuge was used to separate small-diameter fractions. Because the strange and discontinuous behavior of fraction 56 µm was consistent across multiple tests, it is highly likely that most of the dust losses occurred during transportation, lowering the efficiency of this fraction. From a physical point of view, it is impossible that a cyclone separates 100% of the smaller particles and only 80% of the larger particles. Therefore, it was decided to artificially assume

that the efficiency of this fraction was 100%, as it was for fraction 27.7 µm. The fractional separation efficiency for all cases was almost equal to 100% for 8.8 µm. However, measurements show that for this 56 µm fraction, the efficiency was between 94 and 98%. Generally, the CFD model slightly over-predicted the efficiency for the smallest fraction (diameter 1.9 µm) whereas it slightly under-predicts for the following two (i.e., 3.9 µm and 6.4 µm). However, looking at the model, none of the other settings improved these results. Correction of fractional efficiency also increased the total efficiency (see Fig. 14(d)). The differences in global separation efficiency for all three cases showed differences in the range of 0.4–0.7%, which should be considered an acceptable result. The cut-off point for all analyses was located in fraction 8.8 µm and was determined correctly. The differences in results were visible only in the three smallest fractions.

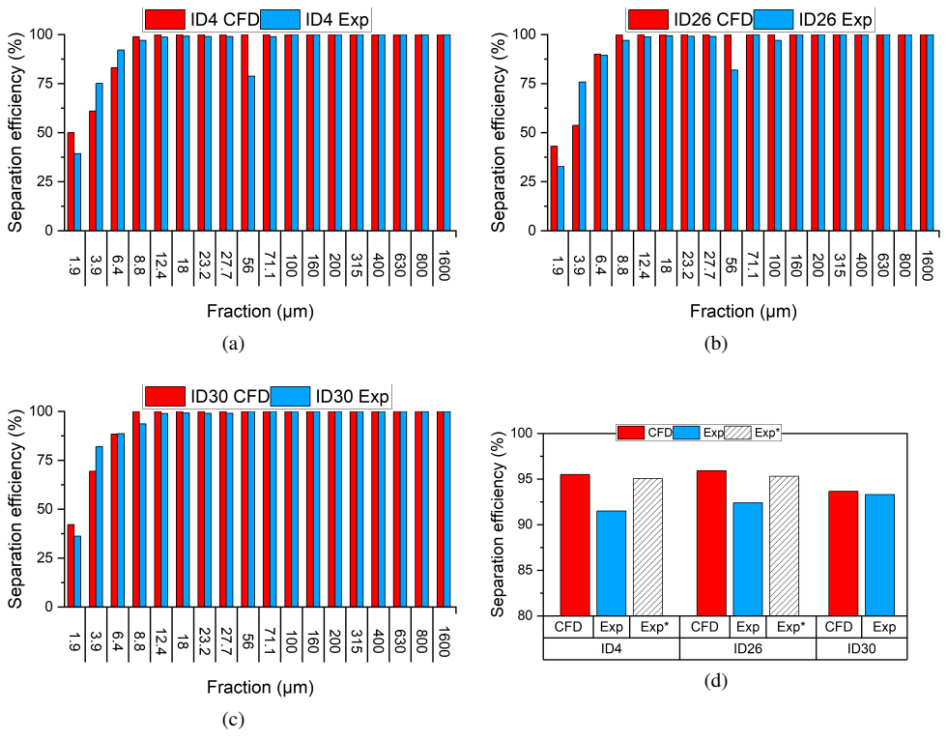

Figure 14: Numerical model validation: a, b, c – fractional separation efficiencies; d – total separation efficiency (CFD – numerical results; Exp – experimental results; Exp* – experimental results assuming 99% separation efficiency of fraction 56 µm in cases ID4 and ID26).

5 Conclusions

The main objective of this study was to develop a numerical model of a cyclone separator for the separation of particulate matter that is able to foresee the cyclone separator cut-off point. This allows for designing of the cyclone separator so the most of the zinc and lead pass through while iron and carbon is removed from gas.

The results of numerical simulation showed good agreement between the numerical results and the experiments for all investigated gas velocities and particle fractions. Only for the smallest particles, the numerical model over-predicted the separation efficiency.

Model accuracy was achieved due to proper selection of the normal and tangential reflection coefficients, which have a significant impact on the separation efficiency. These coefficients were adjusted so that no unfeasible results appeared for any of the dust diameters. In addition, the correct CFN was chosen to stabilize the flow and obtain the correct flow field.

These findings of the pilot-scale cyclone separator analysis will next be used to determine the geometry and flow parameters of a full-scale industrial cyclone separator.

Acknowledgements

This research was supported by the Polish Agency for Enterprise Development within grant no. POIR.01.01.01-00-099/18. Mieszko Tokarski was also supported by the Ministry of Science and Higher Education, Poland, with the grant AGH UST no. 16.16.210.476 and by the NAWA Polish Returns no. 12.12.210.05020 (PPN/PPO/2019/1/00023/U/0001). The publication was supported by statutory research funds of the Faculty of Energy and Environmental Engineering of the Silesian University of Technology.

Received 20 December 2023

References

[1] Lim J.H., Oh S.H., Kang S., Lee K.J., Yook S.J.: *Development of cutoff size adjustable omnidirectional inlet cyclone separator*. Sep. Purif. Technol. **276**(2021), 119397. doi: 10.1016/j.seppur.2021.119397

[2] Babaoglu N.U., Parvaz F., Hosseini S.H., Elsayed K, Ahmadi G.: *Influence of the inlet cross-sectional shape on the performance of a multi-inlet gas cyclone*. Powder Technol. **384**(2021), 82–99. doi: 10.1016/j.powtec.2021.02.008

[3] Wang S., Luo K., Hu C., Fan J.: *CFD-DEM study of the effect of cyclone arrangements on the gas-solid flow dynamics in the full-loop circulating fluidized bed*. Chem. Eng. Sci. **172**(2017), 199–215. doi: 10.1016/j.ces.2017.05.052

[4] Stanek W., Szega M., Blacha L., Niesler M., Gawron M.: *Exergo-ecological assessment of auxiliary fuel injection into blast-furnace*. Arch. Metall. Mater. **60**(2015), 711–719. doi: 10.1515/amm-2015-0196

[5] Li W., Huang Z., Li G., Ye C.: *Effects of different cylinder roof structures on the vortex of cyclone separators*. Sep. Purif. Technol. **296**(2022), 121370. doi: 10.1016/j.seppur.2022.121370

[6] Hsu C.W., Huang S.H., Lin C.W., Hsiao T.C., Lin W.Y., Chen C.C.: *An experimental study on performance improvement of the stairmand cyclone design*. Aerosol Air Qual. Res. **14**(2014), 3, 1003–1016. doi: 10.4209/aaqr.2013.04.0129

[7] Roloff C., Lukas E., Wachem B., Thévenin D.: *Particle dynamics investigation by means of shadow imaging inside an air separator*. Chem. Eng. Sci. **195**(2019), 312–324. doi: 10.1016/j.ces.2018.09.020

[8] Celis G.E.O., Loureiro J.B.R., Lage P.L.C., Silva Freire A.P.: *The effects of swirl vanes and a vortex stabilizer on the dynamic flow field in a cyclonic separator*. Chem. Eng. Sci. **248**(2022), 117099. doi: 10.1016/j.ces.2021.117099

[9] Babaoglu N.U., Hosseini S.H., Ahmadi G., Elsayed K.: *The effect of axial cyclone inlet velocity and geometrical dimensions on the flow pattern, performance, acoustic noise*. Powder Technol. **407**(2022), 117692. doi: 10.1016/j.powtec.2022.117692

[10] Zhang R., Yang J., Han S., Hao X., Guan G.: *Improving advantages and reducing risks in increasing cyclone height via an apex cone to grasp vortex end*. Chin. J. Chem. Eng. **54**(2022), 136–143. doi: 10.1016/j.cjche.2022.04.014

[11] Yoshida H.: *Effect of apex cone shape and local fluid flow control method on fine particle classification of gascyclone*. Chem. Eng. Sci. **85**(2013), 55–61. doi: 10.1016/j.ces.2012.01.060

[12] Yang X., Yang J., Wang S., Zhao Y.: *Effects of operational and geometrical parameters on velocity distribution and micron mineral powders classification in cyclone separators*. Powder Technol. **407**(2022), 117609. doi: 10.1016/j.powtec.2022.117609

[13] Huang A.N., Ito K., Fukasawa T., Yoshida H., Kuo H.P., Fukui K.: *Classification performance analysis of a novel cyclone with a slit on the conical part by CFD simulation*. Sep. Purif. Technol. **190**(2018), 25–32. doi: 10.1016/j.seppur.2017.08.047

[14] Zheng Y., Ni L.: *Numerical study on particles separation using a cyclone enhanced by shunt device: Effects of cylinder-to-cone ratio and vortex finder-to-cylinder ratio*. Powder Technol. **408**(2022), 117767. doi: 10.1016/j.powtec.2022.117767

[15] Pandey S., Brar L.S.: *On the performance of cyclone separators with different shapes of the conical section using CFD*. Powder Technol. **407**(2022), 117629. doi: 10.1016/j.powtec.2022.117629

[16] Martignoni W.P., Bernardo S., Quintani C.L.: *Evaluation of cyclone geometry and its influence on performance parameters by computational fluid dynamics (CFD)*. Braz. J. Chem. Eng. **24**(2007), 83–94. doi: 10.1590/S0104-66322007000100008

[17] Le D.K., Guo M., Yoon J.Y.: *A hybrid CFD – deep learning methodology to improve the accuracy of cut-off diameter prediction in coarse-grid simulations for cyclone separators*. J. Aerosol Sci. **170**(2023), 106143. doi: 10.1016/j.jaerosci.2023.106143

[18] Wasilewski M., Brar L.S.: *Effect of the inlet duct angle on the performance of cyclone separators*. Sep. Purif. Technol. **213**(2019), 19–33. doi: 10.1016/j.seppur.2018.12.023

[19] Xiang R.B., Lee K.W.: *Effects of exit tube diameter on the flow field in cyclones*. Part. Sci. Technol. **26**(2008), 467–481. doi: 10.1080/02726350802367829

[20] Su Y., Zheng A., Zhao B.: *Numerical simulation of effect of inlet configuration on square cyclone separator performance*. Powder Technol. **210**(2011), 293–303. doi: 10.1016/j.powtec.2011.03.034

[21] Azadi M., Azadi M., Mohebbi A.: *A CFD study of the effect of cyclone size on its performance parameters*. J. Hazard. Mater. **182**(2010), 835–841. doi: 10.1016/j.jhazmat.2010.06.115

[22] Oh J., Choi S., Kim J.: *Numerical simulation of an internal flow field in a uniflow cyclone separator*. Powder Technol. **274**(2015), 135–145. doi: 10.1016/j.powtec.2015.01.015

[23] Chen L., Ma H., Sun Z., Ma G., Li P., Li C., Cong X.: *Effect of inlet periodic velocity on the performance of standard cyclone separators*. Powder Technol. **402**(2022), 117347. doi: 10.1016/j.powtec.2022.117347

[24] Zhang L., Chen Y., Zhao B., Dang M., Yao Y.: *Numerical simulation on structure optimization of escape-pipe of cyclone separator with downward outlet*. Powder Technol. **411**(2022), 117588. doi: 10.1016/j.powtec.2022.117588

[25] Slack M.D., Prasad R.O., Bakker A., Boysan F.: *Advances in cyclone modelling using unstructured grids*. Chem. Eng. Res. Des. **78**(2000), 1098–1104. doi: 10.1205/026387600528373

[26] Shalaby H., Wozniak K., Wozniak G.: *Particle-laden flow simulation in a cyclone separator*. Proc. Appl. Math. Mech. **6**(2006), 547–548. doi: 10.1002/pamm.200610254

[27] Dong S., Wang C., Zhang Z., Cai Q., Dong K., Cheng T., Wang B.: *Numerical study of short-circuiting flow and particles in a gas cyclone*. Particuology **72**(2023), 81–93. doi: 10.1016/j.partic.2022.02.008

[28] Guo M., Yang L., Son H., Le D.K., Manickam S., Sun X., Yoon J.Y.: *An overview of novel geometrical modifications and optimizations of gas-particle cyclone separators*. Sep. Purif. Technol. **329**(2024), 125136. doi: 10.1016/j.seppur.2023.125136

[29] Huang L., Yuan J., Pan M., Wu J., Qiao J., Jiang H., Duan C.: *CFD simulation and parameter optimization of the internal flow field of a disturbed air cyclone centrifugal classifier*. Sep. Purif. Technol. **307**(2023), 122760. doi: 10.1016/j.seppur.2022.122760

[30] Stecko J., Stachura R., Niesler M., Bernasowski M., Klimczyk A.: *Utilisation of metallurgical sludge by multi-layer sintering*. Ironmak. Steelmak. **45**(2018), 779–786. doi: 10.1080/03019233.2017.1337285

[31] ANSYS. *Ansys Fluent Theory Guide*. Canonsburg 2019.